Geophysical Journal International

Geophys. J. Int. (2010) **182,** 329–342 doi: 10.1111/j.1365-246X.2010.04609.x

Spatial heterogeneity of tectonic stress and friction in the crust: new evidence from earthquake focal mechanisms in Taiwan

Ya-Ju Hsu,[1] Luis Rivera,[2] Yih-Min Wu,[3] Chien-Hsin Chang[4] and Hiroo Kanamori[5]

[1] *Institute of Earth Sciences, Academia Sinica, Nankang, Taipei* 115*, Taiwan. E-mail: yaru@earth.sinica.edu.tw*
[2] *Institut de Physique du Globe de Strasbourg;* UMR7516*, Université de Strasbourg, CNRS, Strasbourg, France*
[3] *Department of Geosciences, National Taiwan University, Taipei* 106*, Taiwan*
[4] *Central Weather Bureau, Taipei* 100*, Taiwan*
[5] *Seismological Laboratory, California Institute of Technology, CA* 91125*, USA*

Accepted 2010 March 26. Received 2010 March 26; in original form 2009 November 18

SUMMARY

We performed inversions of earthquake focal mechanisms in central Taiwan to investigate the heterogeneity of the stress field and fault strength, and temporal variations of stress parameters, friction and pore pressure associated with the 1999 Chi-Chi earthquake. We divided the focal mechanism data into two groups: before and after the Chi-Chi earthquake, and analysed them separately. With the assumption of a uniform stress field, the friction coefficient is mostly within a range of 0.2–0.4 in central Taiwan, which is lower than the commonly quoted laboratory result, 0.6–0.85. The low friction coefficient is also inferred by the rotation of principal stress axes after the Chi-Chi earthquake. By contrast, if we assume that the friction is constant and failures occur on optimally oriented planes, we find that the resulting stress orientations must be spatially variable. However, a large dispersion of stress orientations is not seen in borehole breakouts and fault slip data, implying a constant friction model might be ruled out. Our analysis suggests that either the distribution of the coefficient of friction or pore pressure changed during the 1999 Chi-Chi earthquake. We infer that the pore pressure probably rose in the Chi-Chi rupture area and northern Longitudinal Valley and dropped in the areas south of the coseismic rupture area after the main shock.

Key words: Permeability and porosity; Friction; Fault zone rheology; Earthquake source observations.

1 INTRODUCTION

Measurements of stress orientations and stress magnitudes are key elements for a better understanding of the tectonic process and earthquake mechanics. Borehole measurements indicate that breakout azimuths at depth are generally aligned with the regional minimum horizontal stress (Bell & Gough 1979; Zoback *et al.* 1985; Brudy *et al.* 1997; Wu *et al.* 2007a), whereas breakout orientations are heterogeneous on active fault zones. Thus, localised breakout rotations may be indicators of recent active faulting (Barton & Zoback 1994; Wu *et al.* 2007a). Breakout directions inferred from a 2-km-deep hole in Taiwan Chelungpu fault drilling project (TCDP) reveal some minor fluctuations of the orientations of maximum horizontal principal stress; this suggests small variability of stress orientations at various depths (Wu *et al.* 2007a). The observed diversity of earthquake focal mechanisms in Taiwan at seismogenic zones also suggests a heterogeneous stress field (Figs 1 and 2). Rivera & Kanamori (2002) analyse focal mechanisms in southern California and conclude that the heterogeneity of stress and/or strength is required to explain a variety of focal mechanisms. On the other hand, investigations on the small-scale faulting at seismogenic depths in the crust suggest that the stress and strength in the crust may be homogeneous on short-to-intermediate length scales (less than a few tens of kilometres), and smoothly varying at longer length scales. Some variability in the inferred stress and strength of small earthquakes may result from measurements errors (Hardebeck 2006). In addition, the general consistency of stress orientations derived from earthquake focal mechanisms and surface strain-rate axes from global positioning system (GPS) velocities in southern California and Taiwan implies that the stress orientations do not significantly vary from the surface to base of the seismogenic zone (Becker *et al.* 2005; Hsu *et al.* 2009b), and the interseismic strain is probably stationary. Measurements on stress orientations in Taiwan from borehole breakout data (Suppe *et al.* 1985) and fault slip data (Angelier *et al.* 1986) also show good agreement with GPS-derived surface strain-rate axes, consistent with expected present-day stress directions.

In this study, we recognize that focal mechanisms may require mild variations of stress and/or strength on small-to-intermediate scales. We examine focal mechanisms based on the two end-member assumptions: first, we assume homogeneity of the stress tensor allowing the friction coefficient to vary from event to event. Second, we assume a constant friction coefficient while allowing for a variable stress tensor. The earthquake focal mechanisms and stress

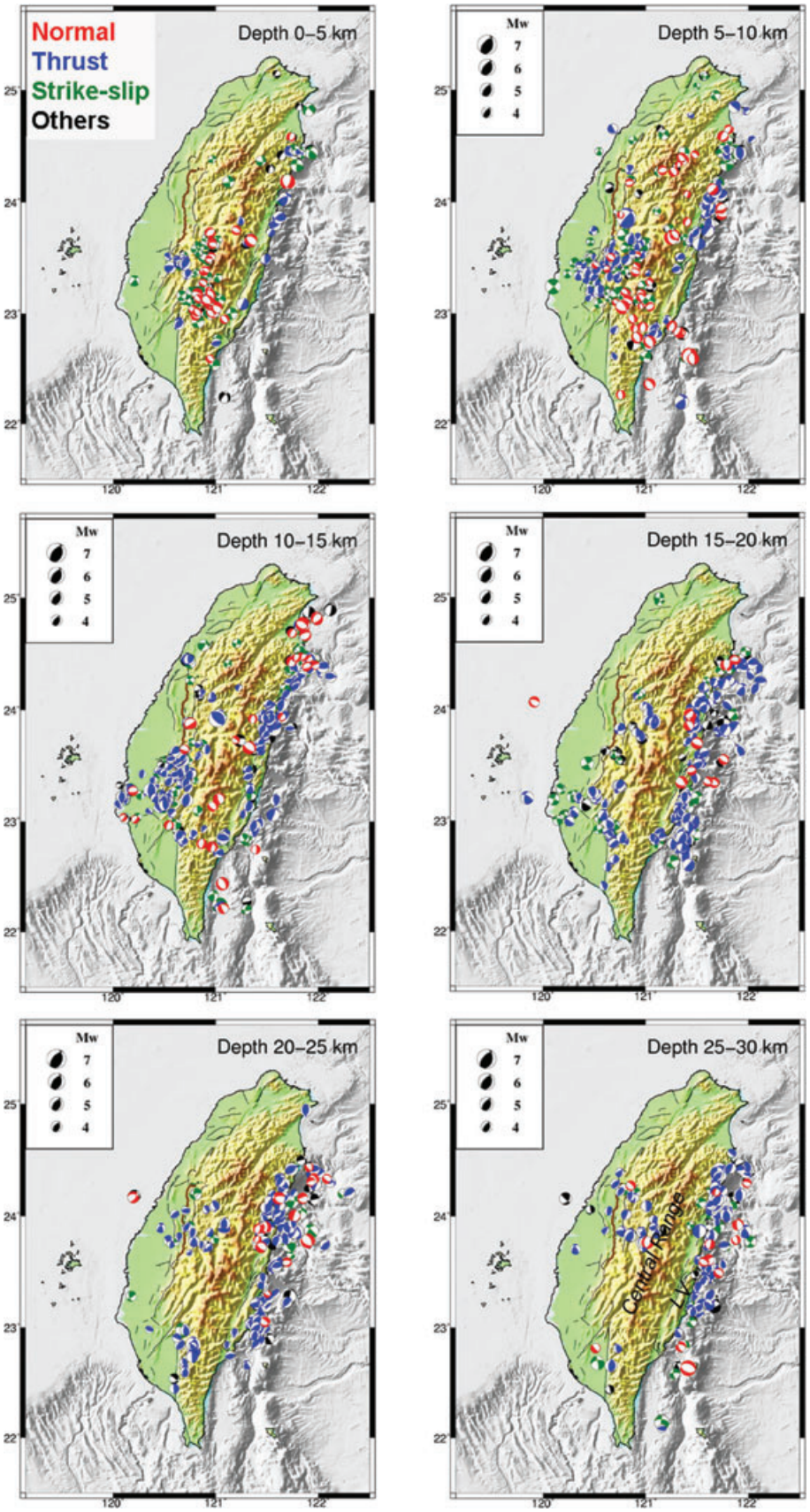

Figure 1. Focal mechanisms at various depth ranges before the 1999 Chi-Chi earthquake. Colour beach balls indicate different fault types shown on top left corner. LV indicates the Longitudinal Valley. Major faults are shown in black lines. The Chelungpu fault is shown in dark brown. Colours indicate the shaded relief topography and bathymetry.

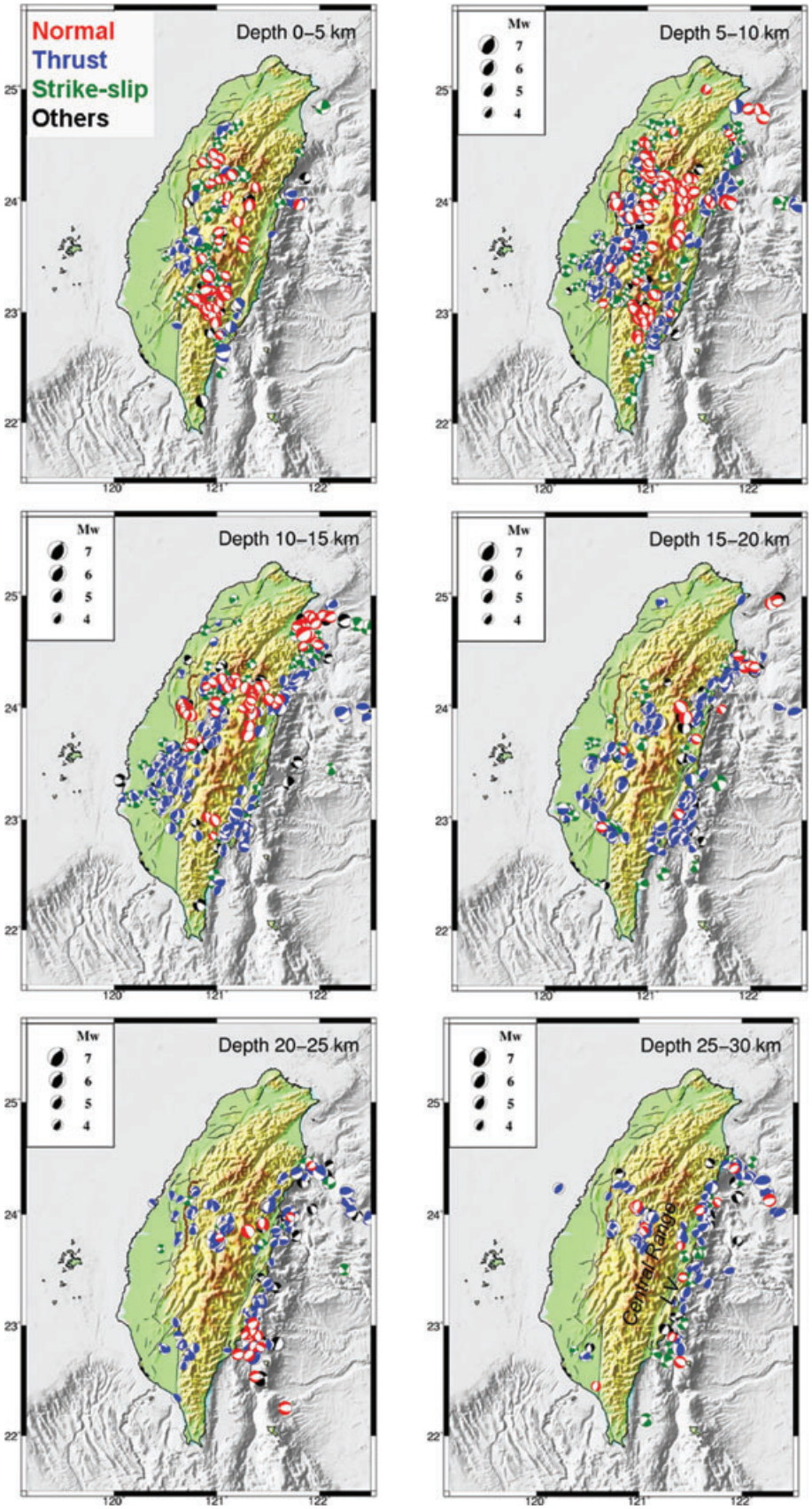

Figure 2. Focal mechanisms at various depth ranges after the 1999 Chi-Chi earthquake. Colour beach balls indicate different fault types shown on top left corner. LV indicates the Longitudinal Valley. Major faults are shown in black lines. The Chelungpu fault is shown in dark brown. Colours indicate the shaded relief topography and bathymetry.

measurements in Taiwan are used to discuss the validity of the two end-member models. We divide central Taiwan into several subdomains according to faulting types and geological setting and perform the analysis for each subdomain. The focal mechanisms before and after the 1999 M_w 7.6 Chi-Chi, Taiwan earthquake are analysed separately. The 1999 earthquake broke the Chelungpu fault and generated more than 100-km-long surface rupture in central Taiwan. It is of interest to know how stress fields responded to the stress perturbation associated with the main shock.

2 DATA

We use earthquake focal mechanisms with magnitude between 2 and 6.8 from the first-motion polarities of P waves (Wu *et al.* 2008; Wu *et al.* 2009). They implemented a genetic algorithm in a non-linear global search to find the best earthquake focal mechanism for the period from 1991 to 2007. In this study, we use the data before (1991–1999.7, Fig. 1) and after (1999.7–2007, Fig. 2) the Chi-Chi earthquake. An alternative choice of earthquake focal mechanism data would be to use those determined from modeling of waveforms recorded with the Broadband Array in Taiwan for Seismology (BATS); however, the number of available solutions for shallow earthquakes (Kao & Jian 2001) is not sufficient for stress-tensor inversions.

In this study, we analyse focal mechanisms in central Taiwan where the crustal stress state is less affected by the two subduction systems to NE and SW of Taiwan. Furthermore, a large number of earthquakes after the Chi-Chi earthquake provide a rare opportunity to study the perturbation of stress state due to a large earthquake. The central Taiwan is divided into four NE-SW trending regions that are consistent with the major structural trend and physiographic regions (Fig. 3). The region covered by Box *A* includes the coastal plain and the western foothills wherein the most coseismic slip occurred during the Chi-Chi earthquake. The region in Box *B* covers the middle section of the Central Range, which is the oldest metamorphic unit in Taiwan. The deformation beneath the Central Range is probably characterised by aseismic slip or ductile flow (Hsu *et al.* 2003). The region in Box *C* contains the northern half of the Longitudinal Valley (LV), which represents the plate suture zone between the Eurasia Plate and the Philippine Sea Plate (Biq 1972; Hsu 1976; Barrier & Angelier 1986; Ho 1986). The Box *D* contains the region to the south of the Chi-Chi coseismic rupture and is considered to be the site of potential future damaging earthquakes. The distribution of focal mechanisms in each region is shown in Fig. 3 by lower-hemisphere projections of P, T and B axes. The average orientation of P axes in most areas is about 110° with the average plunge of 10° in agreement with the plate convergence direction (Fig. 4). In contrast, the average trend of T axes is 50° with the plunge of about 10° on average (Fig. 4). The orientations of P–T axes slightly rotated clockwise in Boxes *A*, *B* and *C* after the Chi-Chi earthquake (Figs 3 and 4). The scatter of P–T axes suggests diversity of focal mechanisms, or measurement errors in determining fault plane solutions. A diverse focal mechanism data set is required for the stress-inversion method to yield a well constrained solution for stress orientation and stress ratio in our study.

The focal mechanisms at depth less than 30 km are divided into four fault types (Fig. 5) including normal, thrust, strike-slip faulting and others (Frohlich 2001). The seismic deformation is mostly caused by thrust and strike-slip faulting in western Taiwan. In central Taiwan, thrust-faulting prevailed before the Chi-Chi earthquake (Figs 1 and 5). In Box *D*, the contributions of strike-slip faulting and thrust faulting are comparable. There are abundant normal faulting events at shallow depths (<15 km) beneath the Central Range (Figs 1 and 5, Box *B*). The LV is characterised by thrust faulting as well as a few strike-slip and normal faulting events at a depth greater than 15 km (Figs 1 and 5, Box *C*). The earthquake focal mechanisms after the Chi-Chi earthquake show pre-dominantly thrust faulting in central Taiwan as well (Fig. 2). The total number of strike-slip and normal fault focal mechanisms also increased significantly after the Chi-Chi earthquake.

3 METHODS AND RESULTS

As mentioned earlier, we discuss the degree of spatial heterogeneity of stress and friction using the approach proposed by Rivera & Kanamori (2002). Their analysis is based on non-dimensional parameters and does not require the knowledge of absolute values of stress. In the first model, we solve for the frictional coefficient on the fault plane of each earthquake using the ratio of shear stress to effective normal stress on the fault plane. The friction coefficient, μ, can be written as

$$\mu = \frac{\sqrt{K_2 - K^2}}{K + S - c\,(2S+1)\,/2} \tag{1}$$

where $K = n_1^2 + n_2^2 R$, $K_2 = n_1^2 + n_2^2 R^2$, $\vec{n} = (n_1, n_2, n_3)$ are the unit normal vector of the fault plane, $R = (\sigma_2 - \sigma_3)/(\sigma_1 - \sigma_3)$, $S = \sigma_3/(\sigma_1 - \sigma_3)$, $c = 2\sigma_p/(\sigma_1 + \sigma_3)$, and σ_p is the pore pressure. Note that n_1, n_2, and n_3 are the components of the vector $\vec{n}$ in the principal axes frame. The stress ratio, R, which gives the ratio of differential stresses is estimated from the stress-tensor inversion. In contrast, the ratio S contains the information about the maximum value of the ratio of shear stress (τ) to normal stress (σ), which is a key parameter pertaining to friction. For a given S, it can be shown that $(\tau/\sigma)_{\max} = \mu_{\max} = 1/2\sqrt{S(1+S)}$ (Appendix A). The value of S can be constrained from the critical taper model and borehole stress measurements. Suppe (2007) inferred the wedge strength of Taiwan, $W = (\sigma_1 - \sigma_3)/\sigma_3$, to be about 0.6, from which $S = 1/W = 1.7$. Suppe (2007) also inferred the value of S to be about 2 using the cohesionless component of the California SAFOD (The San Andreas Fault Observatory at Depth) pilot hole (Hickman & Zoback 2004). In addition, the German KTB (The German Continental Deep Drilling Program) and the Cajon Pass borehole data show that the S value is about 1 (Zoback & Healy 1992; Brudy *et al.* 1997). The stress measurements from TCDP also provide significant constraints and give the value of S about 0.8∼1.1 (Hung *et al.* 2009; Haimson *et al.* 2010). To summarize, these studies suggest that the S value is probably in the range between 1 and ∼2.

The constant c is related to the pore pressure and the mean stress. Given values of S and c in eq. (1), we then estimate friction coefficients. Rivera & Kamanori (2002) give more details of the derivation of eq. (1). Note that we can use different c values according to fault types assuming that the pore pressure is one third of the lithostatic vertical stress (Jaeger 1964). However, considering all the approximations in computations and for simplicity, we decided to use a constant c value of 0.3, which is primarily for strike-slip faulting under hydrostatic pore pressure (Jaeger 1964). We also test the influence of c by varying c values for different fault types. The first-order features of distributions of friction coefficients remain the same.

In the second model, we assume that the friction is constant and failure occurs on an optimally oriented plane. In such case, the intermediate stress axis lies on the fault rupture plane and coincides with the null axis of the focal mechanism (Rivera &

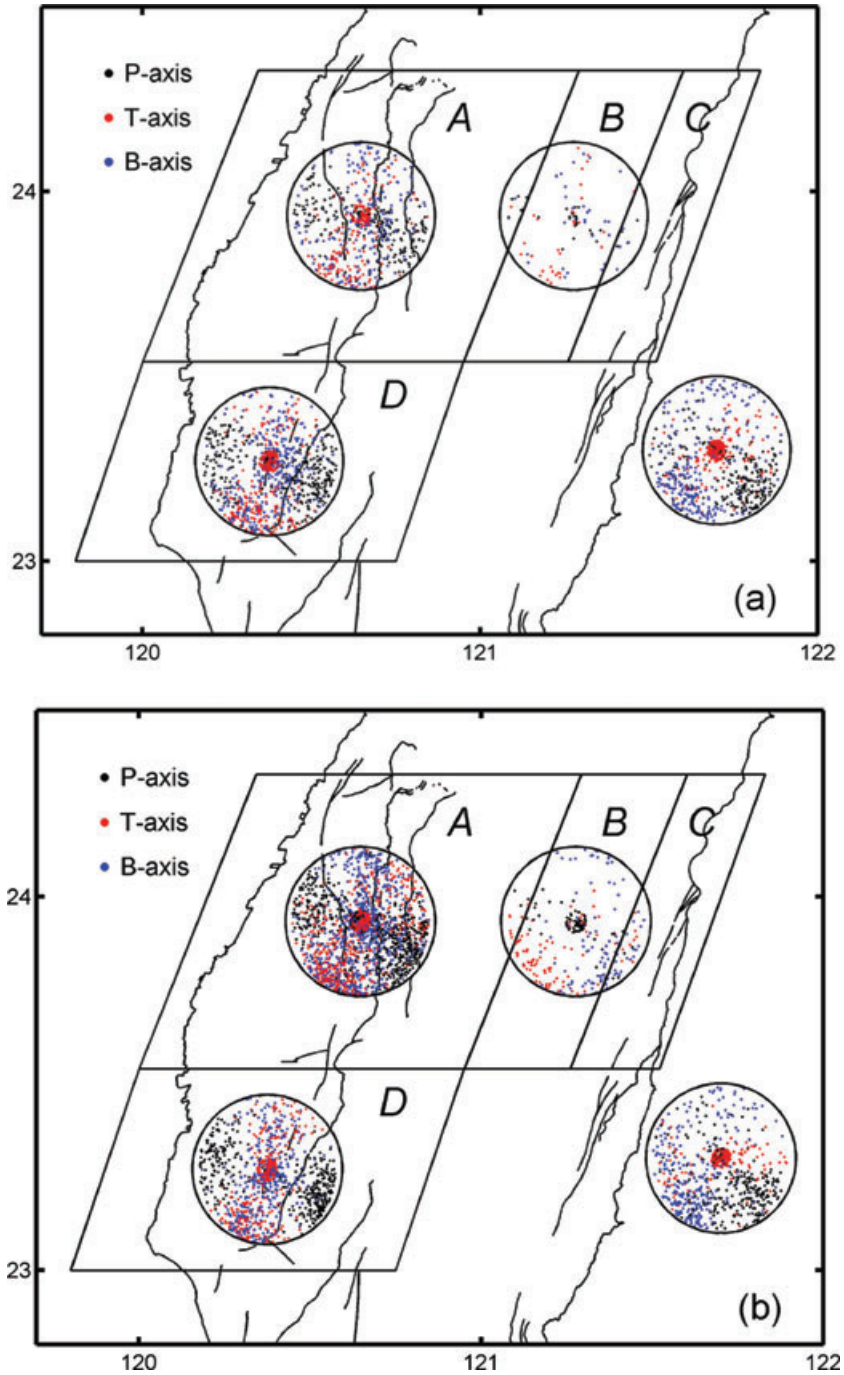

Figure 3. Distributions of P axes (black dots), T axes (red dots), and B (or null) axes (blue dots) of focal mechanisms of earthquakes (Depth <30 km) in each box (a) before and (b) after the Chi-Chi earthquake.

Kanamori 2002). We analyse earthquake focal mechanisms for the periods before (1991–1999.7) and after the Chi-Chi earthquake (1999.7–2007). Results are discussed separately in the following sections.

3.1 'Uniform stress' model

3.1.1 Before the Chi-Chi earthquake

We use the algorithm developed by Michael (1984, 1987) to find the stress tensor that minimizes the difference between the orientation of the shear traction on the fault plane and the fault slip direction for a population of earthquakes. The result is shown in Fig. 5. The mean stress ratios, R, are 0.17, 0.84, 0.29, and 0.29, respectively, in Boxes *A–D* (Fig. 5). The average azimuth of maximum horizontal compressive stress axis (Sh_{azi}) that represents the principal direction of horizontal maximum compressive stress falls in a range of 103°–131° (Fig. 5).

To evaluate error characteristics in stress-tensor inversions, we estimate uncertainties of stress ratio (R) and stress orientations using a bootstrap method (Efron & Tibshirani 1993) by re-sampling actual focal mechanisms to generate 1000 sub-data sets and then

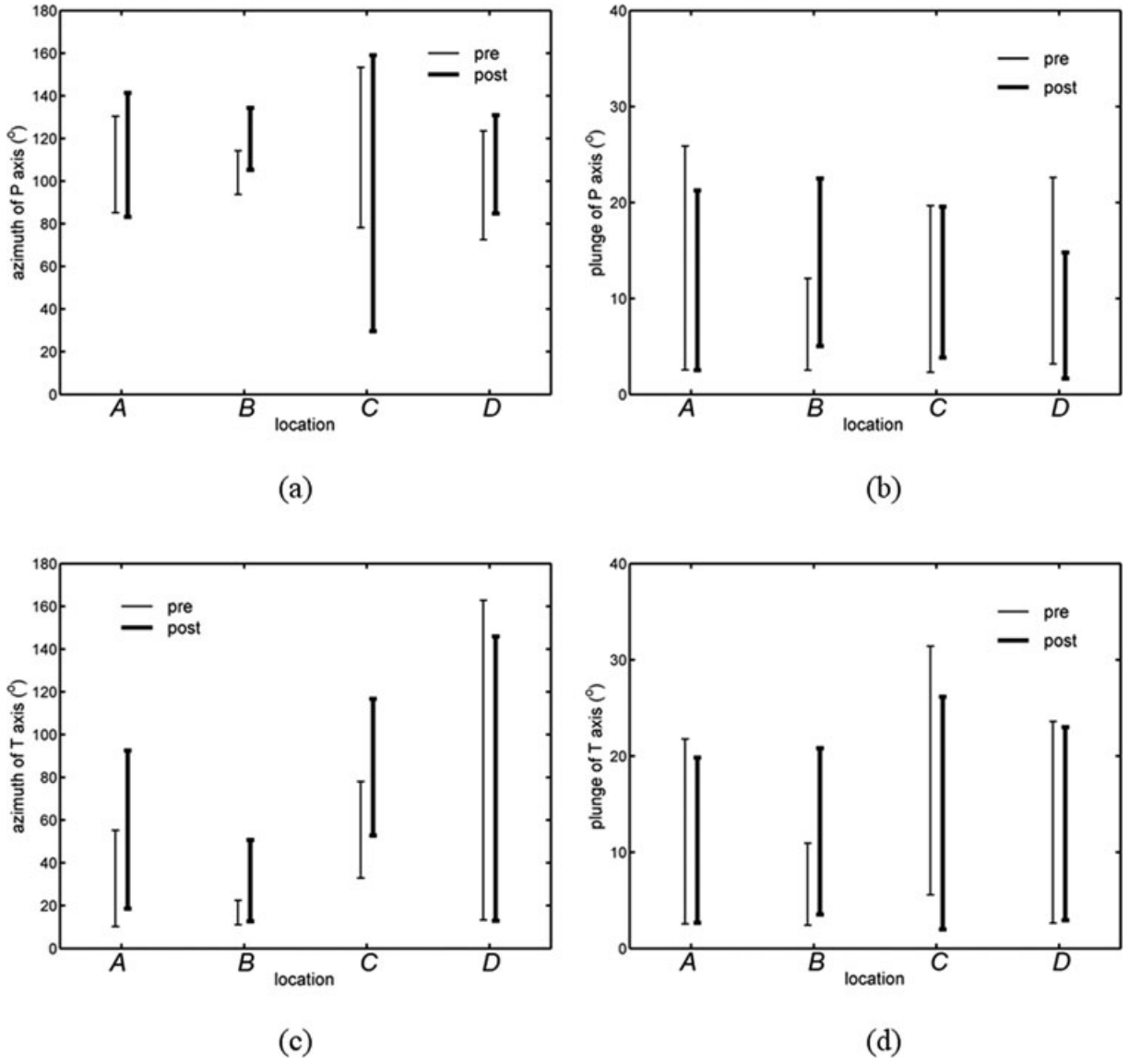

Figure 4. Azimuths and plunges of P–T axes from earthquake focal mechanisms before (thin line) and after (thick line) the Chi-Chi earthquake in four boxes *A–D*. The vertical bars denote the uncertainties of (a) the azimuth and (b) the plunge of P axes and (c) the azimuth and (d) the plunge of T axes.

computing the 67per cent confidence limit of the R value and stress orientations. These uncertainties will be considered later when we compare the results for the periods before and after the Chi-Chi earthquake.

We then compute friction coefficients using eq. (1). We used the unit normal vector ($\vec{n}$) of each earthquake, the stress ratio, R, resulting from the stress-tensor inversions for each box, four values of S ranging from 0.8 to 2.0, and a constant c value of 0.3. Figs 6(a–c) show the distribution of the number of events f_i with friction coefficient μ_i for different values of S from 0.8 to 2. Due to insufficient number of earthquakes in Box B, we do not include the result for Box B in Fig. 6.

In the following discussion, we use two measures of friction as a representative coefficient of friction. First is the average $\bar{\mu}$ that is computed from the distribution shown in Figs 6(a–c) by

$$\bar{\mu} = \frac{\sum_{i=1}^{N} \mu_i f_i}{\sum_{i=1}^{N} f_i} \tag{2}$$

where N is the total number of friction values used.

Second is the mode, μ_M, which is the value of μ corresponding to the peak of the distribution shown in Figs 6(a–c). The values of $\bar{\mu}$ thus computed are in a range between 0.2 and 0.4 irrespective of the S values, as will be shown later in comparison with those obtained for the period after the Chi-Chi earthquake. The horizontal bars in Figs 6(a–c) indicate the range of μ_M corresponding to one standard deviation of R in the stress-tensor inversion for each box. The values of μ_M lie in a range of 0.2–0.5, similar to the distribution of $\bar{\mu}$, in a range of 0.2–0.4.

We have shown earlier that, under the condition of a uniform stress field, μ varies over a fairly large range. However, since there is one free parameter S, a possibility still exists that μ can take a constant value if we adjust the value of S. Thus, we test this possibility as follows. Since μ is often taken constant at 0.6 in the crust (Byerlee 1978), we first examine the variation of S for $\mu = 0.6$ and $c = 0.3$ by solving eq. (1) for S. The numbers of events as a function of S for Boxes A, C and D are shown in Figs 6(d–f). We found that S values are negative for a large number of events. Negative values of S are unacceptable at seismogenic depths. This

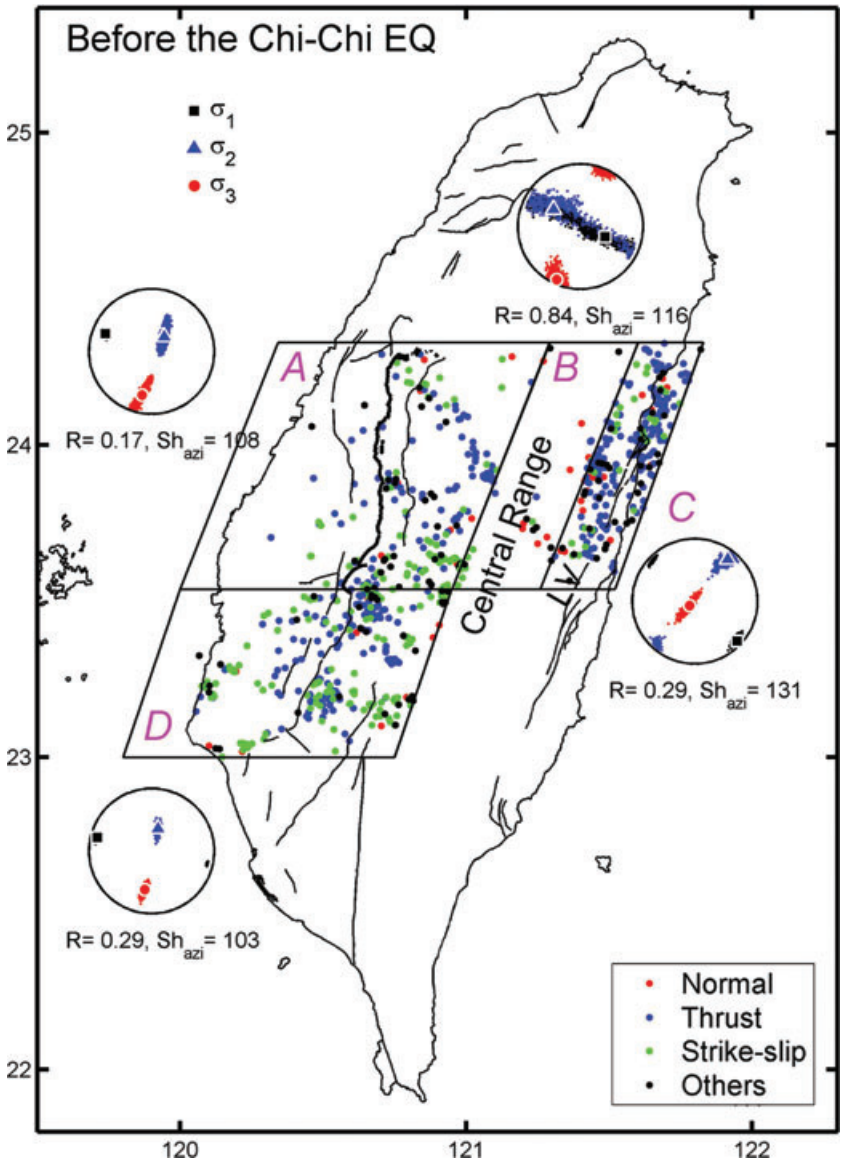

Figure 5. Fault types and stress-tensor inversion results in central Taiwan before the Chi-Chi earthquake. Colour dots denote different fault types shown in bottom right corner. The stress-tensor inversion results in four regions *A–D* are represented by equal-area projection of the lower hemisphere. Squares, triangles and circles represent three principal stress axes σ_1, σ_2, and σ_3. The best solution is marked by large symbols with white outlines. The small symbols show the distribution of stress axes within 95% confidence region. *R* and Sh_{azi} denote the stress ratio $R = (\sigma_2 - \sigma_3)/(\sigma_1 - \sigma_3)$ and the direction of maximum horizontal compressive stress, respectively. The black lines indicate major faults in Taiwan. The Chelungpu fault (CLPF) is shown in thick black line. LV indicates the Longitudinal Valley.

means that no physically meaningful solutions can be found for a large number of events if μ is held constant at 0.6. We then tried different μ and c values and found that a smaller value of μ (e.g. 0.2) and a larger value of c result in more events with positive values of S (Figs 6d–f). However, S values are still negative for nearly half of the total events. These results suggest that under the condition of uniform stress field, given the observed heterogeneity of earthquake mechanisms, the friction coefficient cannot be uniform in the crust.

3.1.2 After the Chi-Chi earthquake

We performed a similar analysis as we did in the previous section using the focal mechanism data of the earthquakes that occurred after the Chi-Chi mainshock. The result of stress inversion is shown in Fig. 7. Note that the number of earthquake focal mechanisms increases by a factor of 3 in Boxes *A* and *B* (Fig. 7) after the Chi-Chi earthquake. Many normal faulting events occurred in Box *B* after the main shock. The mean stress ratios, *R*, are 0.24, 0.55, 0.45, and 0.14, respectively, in Boxes *A–D* (Fig. 7). The average azimuths of the maximum horizontal compressive stress axes, Sh_{azi}, in these regions are in a range of 106°–151° (Fig. 7).

Figs 8(a–c) show the distribution of the number of events f_i with friction coefficient μ_i for different values of S from 0.8 to 2. The values of $\bar{\mu}$ computed with eq. (2) from the distributions shown in Figs 8(a–c) lie in a range between 0.2 and 0.45 irrespective of the S values, as will be shown later in comparison with the result for the period before the Chi-Chi earthquake. The horizontal bars in Figs 8(a–c) indicate the range of μ_M that lies in a range between 0.15 and 0.5.

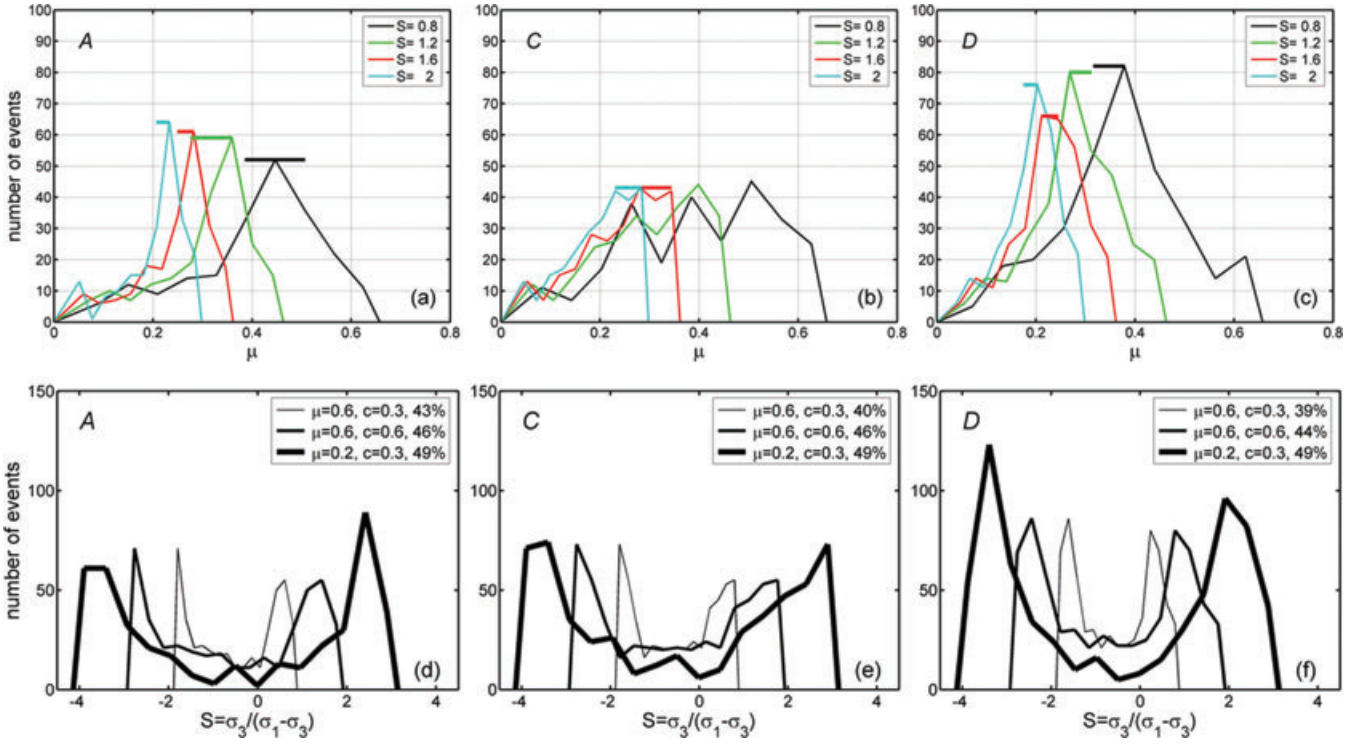

Figure 6. (a–c). The distribution of the number of events as a function of μ for different values of S from 0.8 to 2 before the Chi-Chi earthquake. Horizontal bars show the distributions of the mode μ_M corresponding to one standard deviation of R in stress-tensor inversions. (d–f). The number of events as a function of S value for $\mu = 0.6$ and $c = 0.3$ (grey line). Black lines show the results with different μ and c.

We also examined, for the post-Chi-Chi period, the case in which the friction coefficient is forced to be constant under the uniform stress field. Similar to the case for the pre-Chi-Chi period, about 60per cent of S values estimated with $\mu = 0.6$ and $c = 0.3$ are negative (Figs 8d–f). Using a smaller value of μ, (e.g. 0.2) and a larger value of c results in more events with positive values of S (Figs 8d–f). However, S values are still negative for nearly half of the total events. Thus, under the condition of uniform stress field, given the observed heterogeneity of earthquake mechanisms, the friction coefficient cannot be uniform in the crust.

3.2 'Constant friction' model

We now investigate the other end-member model in which we assume that μ is constant but the orientation of the stress field is allowed to vary. We assume that failure occurs on the optimally oriented faults so that the intermediate stress axis lies on the fault plane. On the basis of this assumption, the orientation of σ_2 axis is parallel to the null axis (B axis) of earthquake focal mechanism (Rivera & Kanamori 2002). We show the orientations of null axes (B axes) in Fig. 3 that are equivalent to the orientations of σ_2 axes. If the null axes are confined in a small range, it suggests that the orientation of the stress field is relatively uniform. In contrast, if the null axes widely spread out, it reflects spatial diversity of the stress field. The null axes show large diversity in the pre- and post-Chi-Chi earthquake period, which suggests that the stress field is heterogeneous.

In this analysis, we assumed that failure occurs on the optimally oriented plane. However, even if we do not make this assumption, the result presented in Section 3.1 shows that if the friction is assumed constant, the stress orientations must spatially vary to explain the large variations of the mechanism solutions. Thus, we conclude that the uniform stress field and the constant friction are in general mutually exclusive.

4 COMPARISON OF THE STRESS FIELD BEFORE AND AFTER THE CHI-CHI EARTHQUAKE

To compare the results for the periods before and after the 1999 Chi-Chi earthquake, we include the confidence limit computed with the bootstrap method mentioned in Section 3.1. Various stress and friction parameters obtained in Section 3.1 are plotted in the following figures for comparison.

Figs 9(a) and (b) compare the stress ratio, R, and the maximum horizontal compressive stress axis, Sh_{azi}, respectively, for the periods before and after the Chi-Chi earthquake. The stress ratio, R, did not change much in Box A, while it decreased after the Ch-Chi earthquake in Boxes B and D and increased in Box C (Fig. 9a). In the pre-Chi-Chi period, the azimuths of σ_2 axis in Box B and σ_1 axis in Box C were parallel to the direction of strain accumulation before the earthquake. The accumulated strain is released after the Chi-Chi mainshock, thus the decrease of R in Box B and the increase of R in Box C may be associated with the decrease of σ_2 in Box B and of σ_1 in Box C, respectively. The maximum horizontal compressive stress axes, Sh_{azi}, systematically rotated by 10°-20° clockwise in Boxes A, B and C after the 1999 earthquake (Fig. 9b).

Fig. 10 shows the comparison of the principal stress axes before and after the Chi-Chi earthquake. Clockwise rotations of about 10°-30° in three principal stress axes are found in all boxes after the main shock, except for the σ_3 axis in Box C. In addition, notable changes of σ_2 axis are shown in Boxes A (azimuth) and B (plunge)

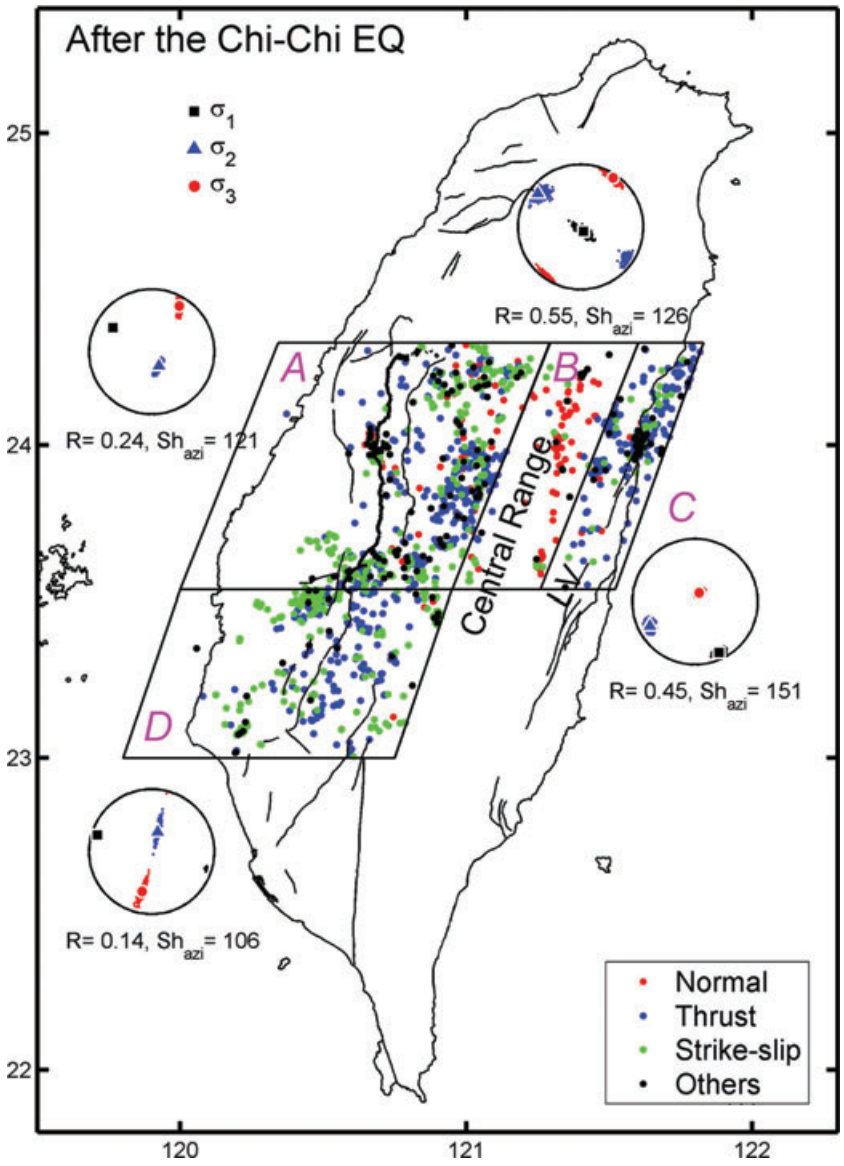

Figure 7. Stress regimes and stress-tensor inversion results in central Taiwan after the Chi-Chi earthquake. Coloured dots denote different fault types shown in bottom right corner. The stress-tensor inversion results in four regions *A*–*D* are represented by equal-area projection of the lower hemisphere. Squares, triangles and circles represent three principal stress axes σ_1, σ_2, and σ_3. The best solution is marked by large symbols with white outlines. The small symbols show the distribution of stress axes within 95% confidence region. *R* and $\mathrm{Sh_{azi}}$ denote the stress ratio $R = (\sigma_2 - \sigma_3)/(\sigma_1 - \sigma_3)$ and the direction of maximum horizontal compressive stress, respectively. The black lines indicate major faults in Taiwan. The Chelungpu fault (CLPF) is shown in thick black line. LV indicates the Longitudinal Valley.

where the stress field was greatly influenced by the coseismic stress perturbation. For the period after the main shock, the average azimuth and plunge of σ_2 in Box *A* are 150° and 65°, respectively; in Box *B*, the average azimuth and plunge of σ_2 are 120° and 10°, respectively. In Box *B*, the orientations of σ_2 axes are distributed within a smaller range in the post-Chi-Chi period compared to those in the pre-Chi-Chi period. To some extent, this may be due to the small number of events in Box *B* before the main shock. The increase of events in Box *B* after the main shock may have provided better constraints on stress-tensor inversions. The variability of σ_2 axis is small in both Boxes *C* and *D* before and after the earthquake. The average azimuth of σ_2 axis is 65° with the average plunge of 10° in Box *C* and the azimuth of σ_2 axis is 20° with the average plunge of 60° in Box *D*. The stress orientations here after the main shock are roughly the same as those in the pre-Chi-Chi period.

Fig. 11 compares the friction coefficient for the period before and after the Chi-Chi earthquake. The vertical bars in Figs 11(a–c) indicate the range of $\bar{\mu}$ corresponding to one standard deviation of *R* in the stress-tensor inversion for each box. The values of $\bar{\mu}$ in Boxes *A* and *C* seem to have decreased after the Chi-Chi earthquake compared with those before the earthquake (Figs 11a and b) whereas the values of $\bar{\mu}$ in Box *D* seem to have increased after the main shock (Fig. 11c). These features are more evident for the mode of μ, μ_M (Fig. 12), than the average, $\bar{\mu}$.

We note, however, that we assumed a constant *c* for the computation of μ. In fact, it is possible that the apparent change in μ can be actually due to the pore pressure change after the earthquake. We can have the same $\bar{\mu}$ before and after the Chi-Chi earthquake, if we increase *c* in Boxes *A* and *C*, and decrease *c* in Box *D*. To show this trend, we show the results with *c* being increased from 0.3 to

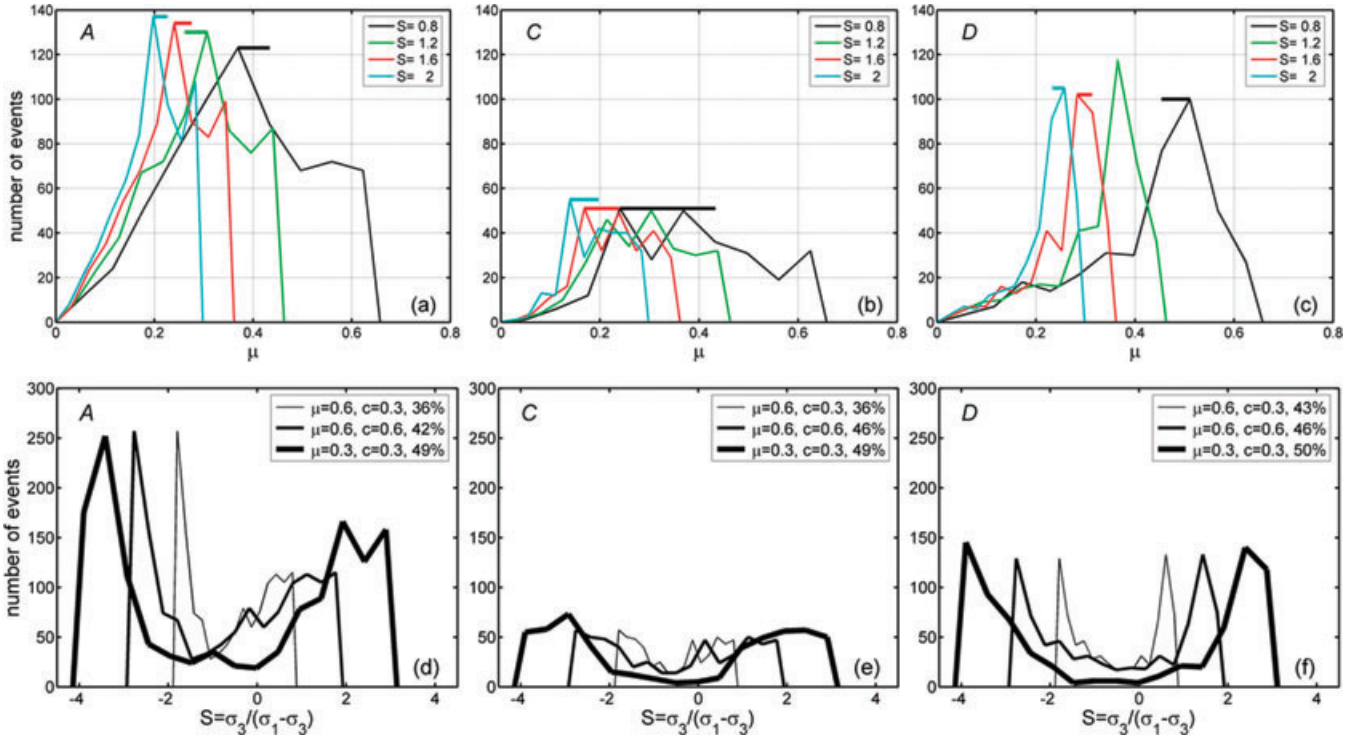

Figure 8. (a–c). The distribution of the number of events as a function of μ for different values of S from 0.8 to 2 after the Chi-Chi earthquake. Horizontal bars show the distributions of the mode μ_M corresponding to one standard deviation of R in stress-tensor inversions. (d–f). The number of events as a function of S value for $\mu = 0.6$ and $c = 0.3$ (grey line). Black lines show the results with different μ and c.

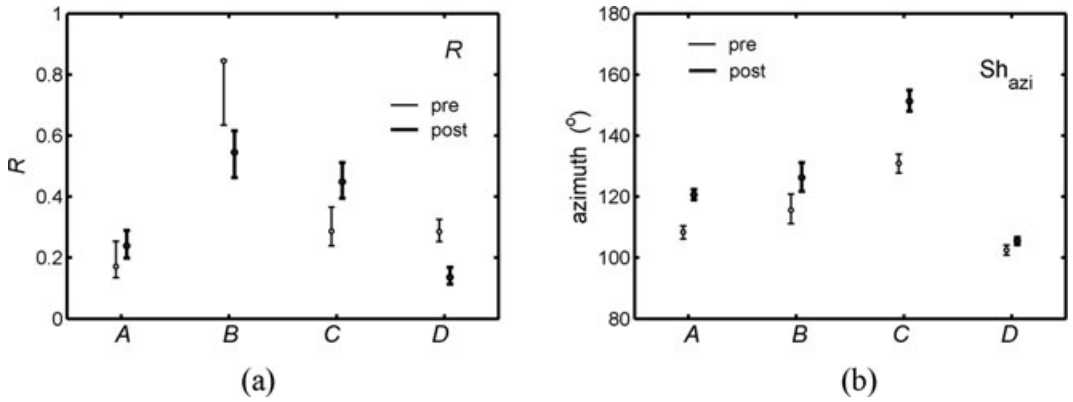

Figure 9. The stress ratio (R) and the azimuth of maximum horizontal compressive stress axis, Sh_{azi}, in the pre- (thin line) and post-Chi-Chi (thick line) periods. The vertical bars show the uncertainty of (a) R and (b) Sh_{azi} in four boxes *A–D.* The optimal solutions are shown as circles.

0.4 for Boxes *A* and *C* (Figs 11d and e, Figs 12d and e). Figs 11(f) and 12(f) show the results for Box *D* where c decreased from 0.3 to 0.2.

5 DISCUSSION

Our results show that if the stress field is assumed uniform, the average friction coefficient must vary over a range from 0.2 to 0.4. If the friction coefficient is forced to be constant, the stress field must vary. A similar conclusion was obtained by Rivera & Kanamori (2002) for earthquakes in southern California. They conclude that uniform stress field and a constant friction are mutually exclusive given the usual variability of focal mechanisms. However, friction coefficients estimated from focal mechanisms in Taiwan show that the values of $\bar{\mu}$ are in a range of 0.2–0.4 with the assumption of a uniform stress field (Figs 11a–c). This concentration of $\bar{\mu}$ values over a wide range of S is not seen in the study of southern California (Rivera & Kanamori 2002). A possible explanation is that the variation of stress orientations is larger in southern California compared to that in Taiwan. However, Hardebeck (2006) found that the variability of the stress orientation and the fault strength is not as large as that suggested by Rivera & Kanamori (2002) if the measurement errors of focal mechanisms are taken into account. In Taiwan, estimates of the orientations of stress axes in the crust- and strain-rate axes derived from the surface GPS velocity field are in good agreement (Chang *et al.* 2003; Hsu *et al.* 2009b). In addition, the stress orientations from borehole breakouts, fault slip data do not show a large variability in stress orientations as required by a constant friction model (Suppe *et al.* 1985; Angelier *et al.* 1986; Hung *et al.* 2009). Based on the constraints from strain and stress

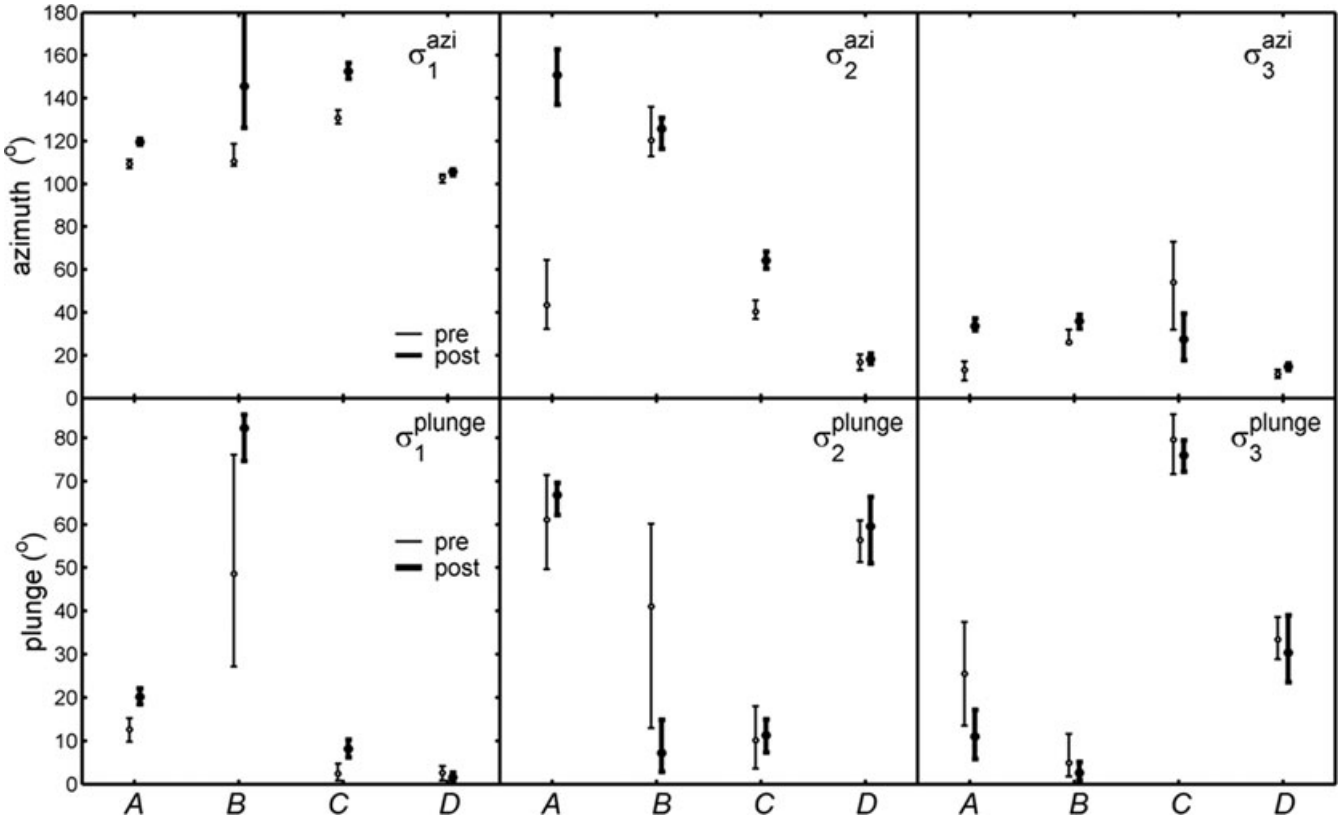

Figure 10. Orientations of principal stress axes derived from stress-tensor inversions before (thin line) and after (thick line) the main shock in four boxes *A–D*. The optimal solutions are shown as circles. The vertical bars denote uncertainties in stress orientations.

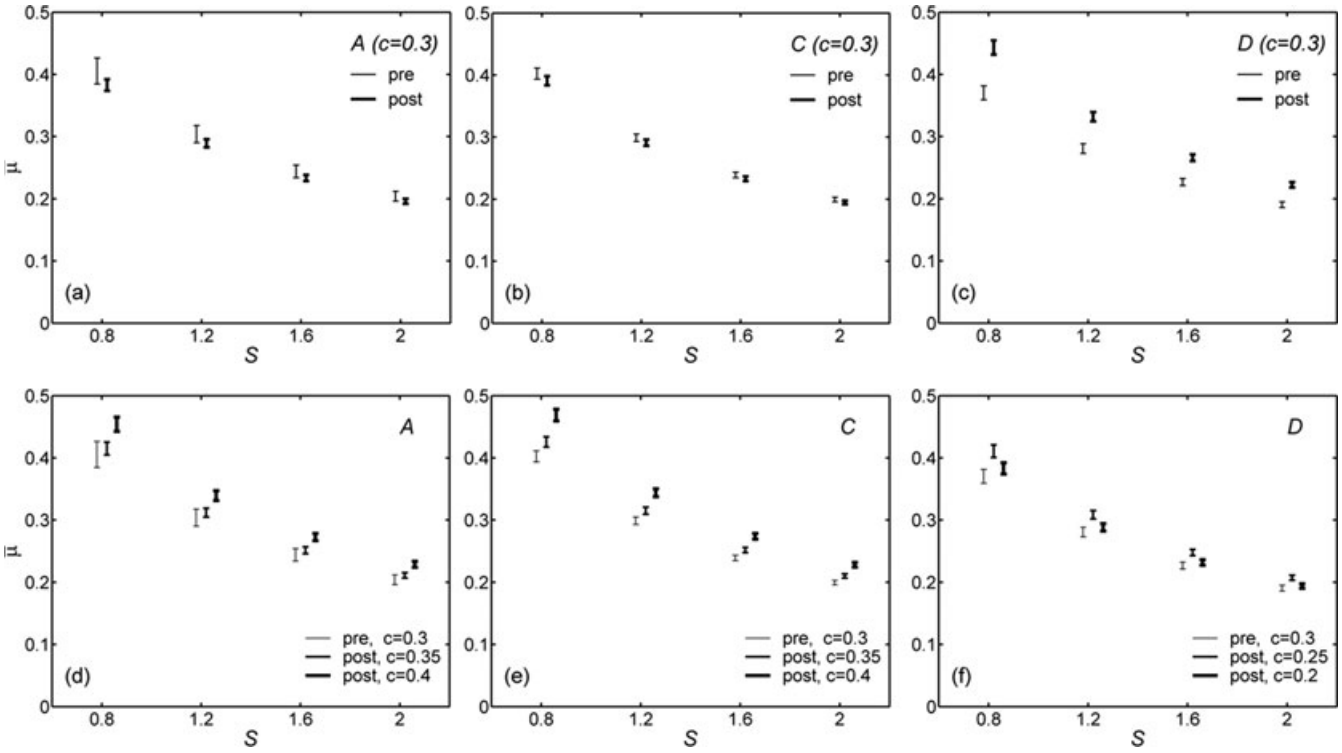

Figure 11. (a–c). The average $\bar{\mu}$ in three boxes (*A*, *C*, *D*) for different values of *S* from 0.8 to 2 before (thin line) and after (thick line) the Chi-Chi earthquake. Vertical bars denote uncertainties of $\bar{\mu}$. (d–f). The average $\bar{\mu}$ for different values of *S* and *c* in the pre- and post-Chi-Chi periods.

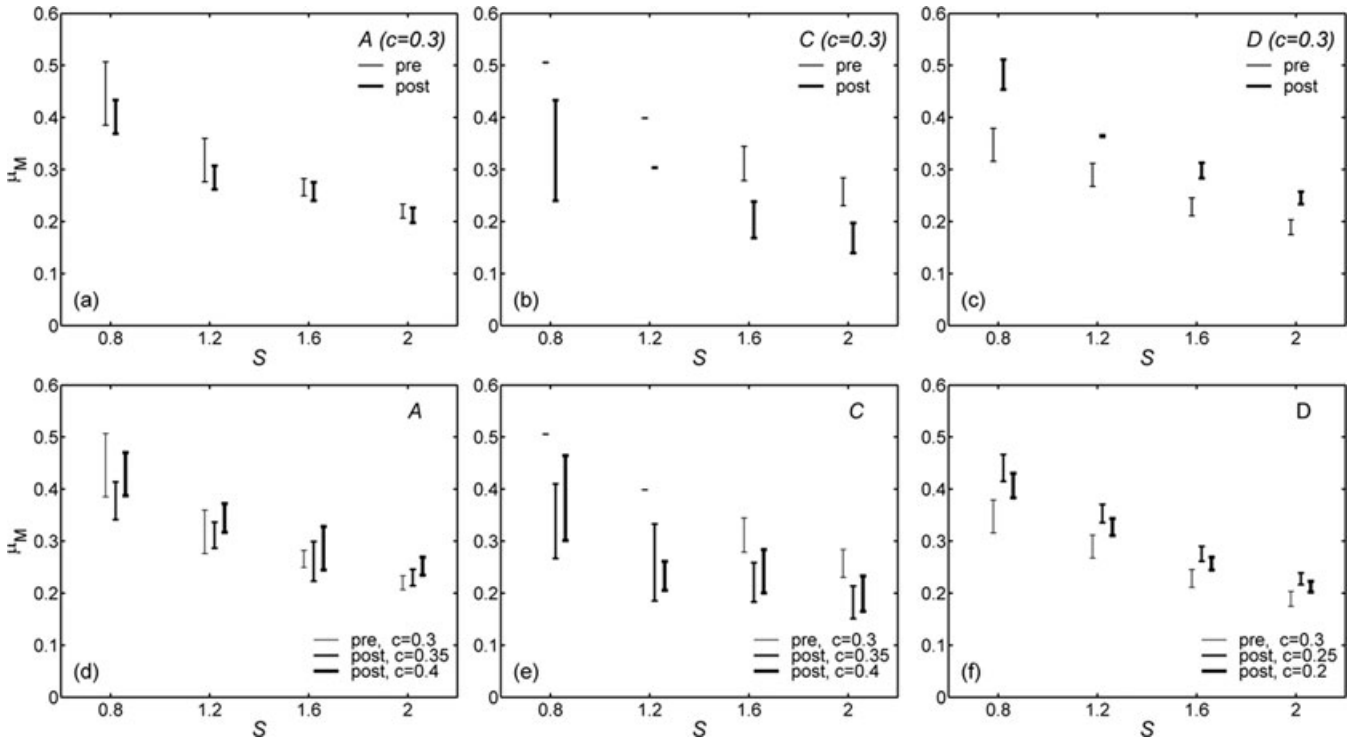

Figure 12. (a–c). The mode μ_M in three boxes (A, C, D) for different values of S from 0.8 to 2 before (thin line) and after (thick line) the Chi-Chi earthquake. Vertical bars denote uncertainties of μ_M. (d–f). The mode μ_M for different values of S and c in the pre- and post-Chi-Chi periods.

measurements in Taiwan, we suggest that a constant friction model is not likely to be the case.

The value of $\bar{\mu}$ lies in a range of 0.2–0.4 (Figs 11a–c) which is lower than the laboratory result of 0.6–0.85; this suggests that the crustal friction in central Taiwan probably does not obey Byerlee's law (1978). We also found that the maximum principal stress axes rotated coseismically (Figs 10a–c). This suggests that the stress magnitude on the fault zone is relatively low so that the relatively small coseismic stress drop of about 1 MPa (Hsu *et al.* 2009a) was large enough to rotate the stress field. This finding agrees with the inferred rotations of fault slip vectors after the main shock (Hsu *et al.* 2009a). In addition, the TCDP reveals only small thermal anomalies in the fault zone and implies a low friction coefficient of 0.04–0.24 (Tanaka *et al.* 2006). Friction experiments using the samples collected from TCDP cores show that the friction coefficient increased from 0.3 to 0.5 with increasing distance from the core of the fault zone to the adjacent country rock (Mizoguchi *et al.* 2008). Furthermore, Suppe (2007) infers that the effective friction coefficient of basal detachment beneath the Taiwan mountain belt is in a range of 0.05–0.1. These results all suggest that the level of friction coefficient is low on the fault zone. The low friction can be caused by fluids, as suggested by Hardebeck & Hauksson (1999) for the San Andreas fault in California. The presence of fluid in central Taiwan is evidenced by various types of data, including the high conductivity measured from magnetotelluric sounding (Chen & Chen 2002), a localised zone with high V_p/Vs ratio at ∼10 km depth beneath the Central Range (Wu *et al.* 2007b) and abundant quartz veins within the Central Range slates (Chan *et al.* 2005).

If we assume that the pore pressure did not change before and after the Chi-Chi earthquake, we find that the friction coefficients changed before and after the earthquake. The apparent change in friction coefficient, especially the large increase in $\bar{\mu}$ and μ_M in Box D, can be alternatively interpreted as a result of change in pore pressure. If we are to have the same $\bar{\mu}$ and μ_M before and after the Chi-Chi earthquake, the c value has to be increased by 0.05 to 0.1 in Boxes A and C and decreased by 0.1 in Box D (Figs 11d–f, Figs 12d–f). This result suggests that the pore pressure possibly rose in Boxes A and C and dropped in Box D in the post-Chi-Chi period. Although these changes are only marginally significant considering the uncertainties in the stress-tensor inversions, the large change in $\bar{\mu}$ and μ_M in Box D could be due to rupture of the Chi-Chi earthquake that may have created fractures in fluid-overpressured portions of the fault zone in Box D. As a result, isolated pore fluids may have flown to equilibrate pore pressure and partially reduce the pore pressure in Box D.

6 CONCLUSIONS

We suggest that a constant friction model is not likely to be the case in Taiwan. The stress inversion study shows that, under the assumption of uniform stress field and for a wide range of the ratio, S, of the minimum stress to the differential stress, the average coefficient of friction, $\bar{\mu}$, in central Taiwan ranges from 0.2 to 0.4. Our data suggest that the stress axes rotated at the time of the 1999 Chi-Chi earthquake, from which we infer that the fault strength is weak. The weak fault is most likely a result of the high fluid pressure in the fault zone. We also found evidence that the pore pressure possibly rose in the rupture area and the northern LV and dropped in the region south of the 1999 Chi-Chi rupture zone after the earthquake.

ACKNOWLEDGMENTS

We thank the Editor, Dr. I. Grevemeyer, and the two reviewers, Dr. S. Ghimire and Dr. J. Suppe for their thoughtful reviews and

valuable comments that helped to improve the manuscript. This study is supported by the Institute of Earth Sciences, Academia Sinica, the National Science Council of the Republic of China grant NSC 98-2119-M-001-033-MY3. This is a contribution of the Institute of Earth Sciences, Academia Sinica, IESASXXX.

REFERENCES

Angelier, J., Barrier, E. & Chu, H.T., 1986. Plate collision and paleostress trajectories in a fold thrust belt—the foothills of Taiwan, *Tectonophysics,* **125,** 161–178.

Barrier, E. & Angelier, J., 1986. Active collision in eastern Taiwan—the Coastal Range, *Tectonophysics,* **125,** 39–72.

Barton, C.A. & Zoback, M.D., 1994. Stress perturbations associated with active faults penetrated by boreholes—possible evidence for near-complete stress drop and new technique for stress magnitude measurement, *J. geophys. Res.,* **99,** 9373–9390.

Becker, T.W., Hardebeck, J.L. & Anderson, G., 2005. Constraints on fault slip rates of the southern California plate boundary from GPS velocity and stress inversions, *Geophys. J. Int.,* **160,** 634–650.

Bell, J.S. & Gough, D.I., 1979. Northeast-southwest compressive stress in Albetra—evidence from oil wells, *Earth planet. Sci. Lett.,* **45,** 475–482.

Biq, C.C., 1972. Dual trench structure in the Taiwan-Luzon region, *Proc. Geol. Soc. China,* **15,** 65–75.

Brudy, M., Zoback, M.D., Fuchs, K., Rummel, F. & Baumgartner, J., 1997. Estimation of the complete stress tensor to 8 km depth in the KTB scientific drill holes: implications for crustal strength, *J. geophys. Res.,* **102,** 18453–18475.

Byerlee, J., 1978. Friction of rocks, *Pure appl. Geophys.,* **116,** 615–626.

Chan, Y.C., Okamoto, K., Yui, T.F., Iizuka, Y. & Chu, H.T., 2005. Fossil fluid reservoir beneath a duplex fault structure within the Central Range of Taiwan: implications for fluid leakage and lubrication during earthquake rupturing process, *TerraNova,* **17,** 493–499.

Chang, C.P., Chang, T.Y., Angelier, J., Kao, H., Lee, J.C. & Yu, S.B., 2003. Strain and stress field in Taiwan oblique convergent system: constraints from GPS observation and tectonic data, *Earth planet. Sci. Lett.,* **214,** 115–127.

Chen, C.C. & Chen, C.S., 2002. Sanyi-Puli conductivity anomaly in NW Taiwan and its implication for the tectonics of the 1999 Chi-Chi earthquake, *Geophys. Res. Lett.,* **29,** doi:10.1029/2001GL013890

Efron, B. & Tibshirani, R.J., 1993. *An Introduction to the Bootstrap,* 436 pp., Chapman and Hall, New York.

Frohlich, C., 2001. Display and quantitative assessment of distributions of earthquake focal mechanisms, *Geophys. J. Int.,* **144,** 300–308.

Haimson, B., Lin, W., Oku, H., Hung, J.H. & Song, S.R., 2010. Integrating borehole-breakout dimensions, strength criteria, and leak-off test results, to constrain the state of stress across the Chelungpu Fault, Taiwan, *Tectonophysics,* **482,** 65–72.

Hardebeck, J.L. & Hauksson, E., 1999. Role of fluids in faulting inferred from stress field signatures, *Science,* **285,** 236–239.

Hardebeck, J.L., 2006. Homogeneity of small-scale earthquake faulting, stress, and fault strength, *Bull. seism. Soc. Am.,* **96,** 1675–1688.

Hickman, S. & Zoback, M., 2004. Stress orientations and magnitudes in the SAFOD pilot hole, *Geophys. Res. Lett.,* **31,** doi:10.1029/2004GL020043

Ho, C.S., 1986. A synthesis of the geologic evolution of Taiwan, *Tectonophysics,* **125,** 1–16.

Hsu, T.L., 1976. Neotectonics of the Longitudinal Valley, eastern Taiwan, *Bull. Geol. Surv. Taiwan,* **25,** 53–62.

Hsu, Y.J., Simons, M., Yu, S.B., Kuo, L.C. & Chen, H.Y., 2003. A two-dimensional dislocation model for interseismic deformation of the Taiwan mountain belt, *Earth planet. Sci. Lett.,* **211,** 287–294.

Hsu, Y.J., Avouac, J.P., Yu, S.B., Chan, C.H., Wu, Y.M. & Woessner, J., 2009a. Spatio-temporal slip, and stress level on the faults within the western foothills of Taiwan: implications for fault frictional properties, *Pure appl. Geophys.,* **166,** 1853–1884.

Hsu, Y.J., Yu, S.B., Simons, M., Kuo, L.C. & Chen, H.Y., 2009b. Interseismic crustal deformation in the Taiwan plate boundary zone revealed by GPS observations, seismicity, and earthquake focal mechanisms, *Tectonophysics,* **479,** 4–18.

Hung, J.H., Ma, K.F., Wang, C.Y., Ito, H., Lin, W.R. & Yeh, E.C., 2009. Subsurface structure, physical properties, fault-zone characteristics and stress state in scientific drill holes of Taiwan Chelungpu Fault Drilling Project, *Tectonophysics,* **466,** 307–321.

Jaeger, J.C., 1964. *Elasticity, Fracture and Flow,* 2nd edn, 212 pp., Methuen & Co., London.

Kao, H. & Jian, P.R., 2001. Seismogenic patterns in the Taiwan region: insights from source parameter inversion of BATS data, *Tectonophysics,* **333,** 179–198.

Michael, A.J., 1984. Determination of stress from slip data—faults and folds, *J. geophys. Res.,* **89,** 1517–1526.

Michael, A.J., 1987. Use of focal mechanisms to determine stress—a control study, *J. geophys. Res.,* **92,** 357–368.

Mizoguchi, K., Takahashi, M., Tanikawa, W., Masuda, K., Song, S.R. & Soh, W., 2008. Frictional strength of fault gouge in Taiwan Chelungpu fault obtained from TCDP Hole B, *Tectonophysics,* **460,** 198–205.

Rivera, L. & Kanamori, H., 2002. Spatial heterogeneity of tectonic stress and friction in the crust, *Geophys. Res. Lett.,* **29,** doi:10.1029/2001GL013803.

Suppe, J., Hu, C.T. & Chen, Y.J., 1985. Preset-day stress directions in western Taiwan inferred from borehole elongation, *Petrol. Geol. Taiwan,* **21,** 1–12.

Suppe, J., 2007. Absolute fault and crustal strength from wedge tapers, *Geology,* **35,** 1127–1130.

Tanaka, H., Chen, W.M., Wang, C.Y., Ma, K.F., Urata, N., Mori, J. & Ando, M., 2006. Frictional heat from faulting of the 1999 Chi-Chi, Taiwan earthquake, *Geophys. Res. Lett.,* **33,** doi:10.1029/2006GL026673.

Wu, H.Y., Ma, K.F., Zoback, M., Boness, N., Ito, H., Hung, J.H. & Hickman, S., 2007a. Stress orientations of Taiwan Chelungpu-Fault Drilling Project (TCDP) hole-A as observed from geophysical logs, *Geophys. Res. Lett.,* **34,** doi:10.1029/2006GL028050.

Wu, Y.M., Chang, C.H., Zhao, L., Shyu, J.B.H., Chen, Y.G., Sieh, K. & Avouac, J.P., 2007b. Seismic tomography of Taiwan: improved constraints from a dense network of strong motion stations, *J. geophys. Res.,* **112,** doi:10.1029/2007JB004983.

Wu, Y.M., Zhao, L., Chang, C.H. & Hsu, Y.J., 2008. Focal-mechanism determination in Taiwan by genetic algorithm, *Bull. seism. Soc. Am.,* **98,** 651–661.

Wu, Y.M., Hsu, Y.J., Chang, C.H., Teng, L.S. & Nakamura, M., 2009. Stress pattern changes in Taiwan from 1991 to 2007: insights from comprehensive first motion focal mechanism catalog, *Earth planet. Sci. Lett.,* submitted.

Zoback, M.D., Moos, D., Mastin, L. & Anderson, R.N., 1985. Well bore breakouts and in situ stress, *J. geophys. Res.,* **90,** 5523–5530.

Zoback, M.D. & Healy, J.H., 1992. In situ stress measurements to 3.5 km depth in the Cajon Pass scientific research borehole: implications for the mechanics of crustal faulting, *J. geophys. Res.,* **97,** 5039–5057.

APPENDIX A: THE STRESS RATIOS *R*, *S* AND MOHR'S CIRCLE

From the definition of R and S, we can write $\sigma_1 = \sigma_3(1 + \frac{1}{S})$ and $\sigma_2 = \sigma_3(1 + \frac{R}{S})$. Thus we can construct a Mohr's circle as shown in Fig. A1. We know $\overline{PC} = (\sigma_1 - \sigma_3)/2 = (\sigma_3/2S)$ and $\overline{OC} = \sigma_3 + \overline{PC} = \sigma_3(1 + \frac{1}{2S})$. Thus the maximum of the ratio, $(\tau/\sigma_n)_{\max} = \mu_{\max}$, can be given by

$$\frac{\overline{PQ}}{\overline{OQ}} = \frac{\overline{PC}}{\overline{OP}} = \frac{\overline{PC}}{\sqrt{\overline{OC}^2 - \overline{PC}^2}} = \frac{1}{2\sqrt{S(1+S)}}$$

Notice that the values of σ_3 and $(\sigma_1 - \sigma_3)$ appear only on the intermediary steps. The final value of $(\tau/\sigma_n)_{\max}$ depends only on S and is in particular independent of the absolute values of stress. Fig. A1 is shown for the case where $\sigma_p = 0$, but it can be extended to the case where $\sigma_p \neq 0$ by moving the origin O by σ_p to the right.

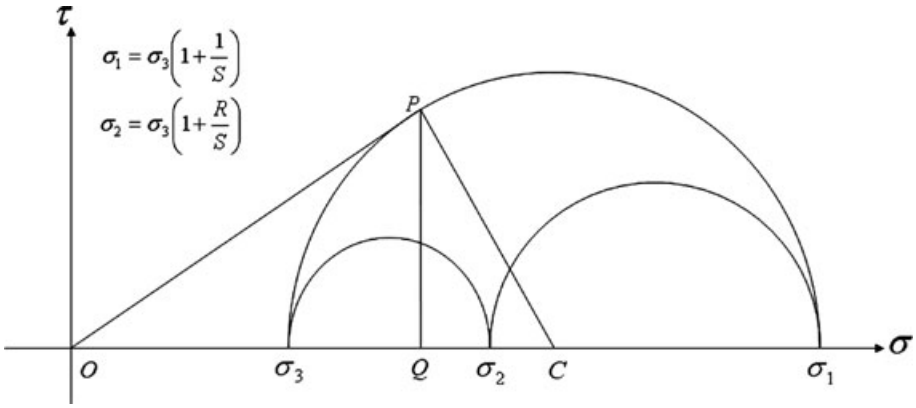

Figure A1. Mohr's diagram of principal stress and stress ratios R and S